Instrumented elephant seals reveal the seasonality in chlorophyll and light-mixing regime in the iron-fertilized Southern Ocean

Stéphane Blain, Sophie Renaut, Xiaogang Xing, Hervé Claustre, Christophe Guinet

Instrumented elephant seals reveal the seasonality in chlorophyll and light-mixing regime in the iron-fertilized Southern Ocean

Stéphane Blain,[1,2] Sophie Renaut,[1,2] Xiaogang Xing,[3,4] Hervé Claustre,[3,4] and Christophe Guinet[5]

Received 19 September 2013; revised 28 November 2013; accepted 2 December 2013; published 19 December 2013.

[1] We analyze an original large data set of concurrent in situ measurements of fluorescence, temperature and salinity provided by sensors mounted on the elephant seals of Kerguelen Island. Our results were mainly gathered in regions of the Southern Ocean where the typical iron limitation is relieved by natural iron fertilization. Thus the role of light as the proximal factor of control of phytoplankton can be examined. We show that self-shading, and consequently stratification, are major factors controlling the integrated biomass during the bloom induced by iron fertilization. When the mixed layer was the shallowest, the maximum Chl_{ML} achievable by the given light-mixing regime was however not reached, most likely due to silicic acid limitation. We also show that a favorable light-mixing regime prevails after the spring equinox and is maintained for roughly seven months (October–April). **Citation:** Blain, S., S. Renaut, X. Xing, H. Claustre, and C. Guinet (2013), Instrumented elephant seals reveal the seasonality in chlorophyll and light-mixing regime in the iron-fertilized Southern Ocean, *Geophys. Res. Lett.*, *40*, 6368–6372, doi:10.1002/2013GL058065.

1. Introduction

[2] Seasonality is a major characteristic of the temporal evolution for marine ecosystems at high latitudes. Salinity, heat fluxes, and wind stress alter the stratification of the upper ocean with modifications of light and nutrients which support growth of phytoplankton. The Southern Ocean mixed layer is very sensitive to climate variability, but the consequences for the dynamics of phytoplankton blooms are controversial [*Lovenduski and Gruber*, 2005; *Sallée et al*., 2010]. Resolving this issue is crucial because phytoplankton blooms impact the magnitude of the biological pump of CO_2 [*Marinov et al*., 2006], and they sustain a unique marine food web. In the Southern Ocean, the general oceanic circulation supplies the enlightened surface layer with nutrients and CO_2-rich waters. During the northward transport of these waters, phytoplankton only consumes a fraction of the available nutrients, allowing CO_2 to escape to the atmosphere. This CO_2 leakage significantly impacts climate [*Sigman et al*., 2010]. The inefficient functioning of the biological pump of CO_2 in the Southern Ocean is mainly attributed to iron limitation of phytoplankton. This was clearly demonstrated by both artificial iron fertilization experiments [*Boyd et al*., 2007; *Smetacek et al*., 2012] and investigations in naturally iron-fertilized regions [*Blain et al*., 2007; *Pollard et al*., 2009]. However, all these experiments were conducted during summer when the mixed layer is the shallowest [*Boyd et al*., 2007]. In the Southern Ocean the stratification of the upper water column is relatively weak compared to low-latitude waters, and during most of the year strong winds contribute to create deep mixed layers potentially unfavorable for phytoplankton growth [*Boyd*, 2002].

[3] During the past decade, our knowledge of the temporal and spatial variability of the mixed layer depth (MLD) in the Southern Ocean was greatly improved by in situ measurements of temperature, salinity, and pressure with autonomous sensors mounted on Argo floats [*Sallée et al*., 2010] or elephant seals [*Charrassin et al*., 2008]. Robust climatologies of the MLD are now available, which show how climate variability (e.g., southern annular mode) impacts the MLD [*Sallée et al*., 2010]. The spatial and temporal variability of phytoplankton biomass is estimated from remote-sensed ocean color [*Arrigo et al*., 2008; *Allison et al*., 2010]. Satellite-derived products have also been used to study the physiological responses of phytoplankton during iron fertilization [*Westberry et al*., 2013]. However, concurrent in situ MLD and chlorophyll data covering the entire annual cycle for a large region are still missing, hampering our further understanding of the effect of the light-mixing regime on the dynamics of phytoplankton blooms.

[4] The southern elephant seals (*Mirounga Leonina*) are deep-diving predators that spend several months at sea in all different provinces of the Southern Ocean, from the sea ice zone to subtropical waters (Figure 1). In previous studies, instrumented southern elephant seals have provided valuable data for studying frontal structures and sea ice formation rates [*Charrassin et al*., 2008]. In our study we used these animals to get insight into the seasonality of chlorophyll and light-mixing regime.

2. Material and Methods

2.1. Deployment and Calibration of Sensors

[5] The data were collected by 23 elephant seals (*Mirounga Leonina*) of the Kerguelen Island. The tags were deployed

Additional supporting information may be found in the online version of this article.

[1]Laboratoire d'Océanographie Microbienne, Université de Paris 06, Banyuls sur mer, France.
[2]Laboratoire d'Océanographie Microbienne, CNRS, Banyuls sur mer, France.
[3]Laboratoire d'Océanographie de Villefranche, Université de Paris 06, Villefranche-sur-Mer, France.
[4]Laboratoire d'Océanographie de Villefranche, CNRS, Villefranche-sur-Mer, France.
[5]Centre d'Etudes Biologiques de Chizé, CNRS, Villiers-en-Bois, France.

Corresponding author: S. Blain, Laboratoire d'Océanographie Microbienne, Université de Paris 06, Avenue du Fontaulé, Banyuls sur mer, FR-66650, France. (stephane.blain@obs-banyuls.fr)

0094-8276/13/10.1002/2013GL058065

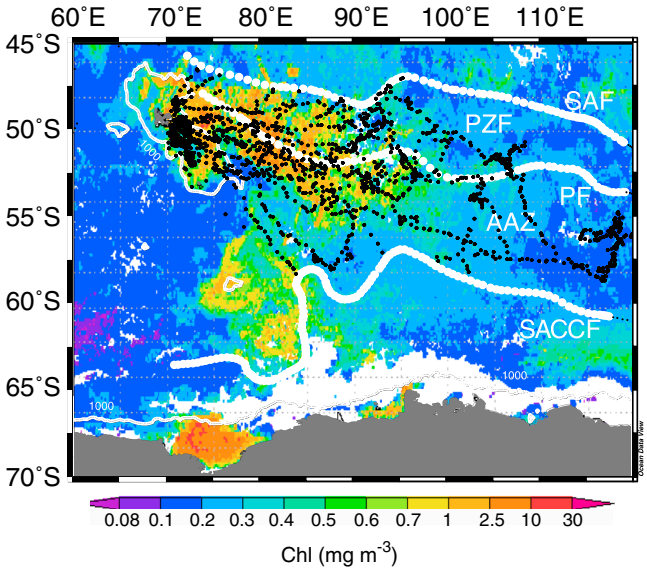

Figure 1. Map of the studied area. Black circles denote the positions of the vertical profiles sampled by elephant seals in the iron-fertilized regions. Others profiles collected north of the PF, South of SACCF, and west of the Kerguelen Plateau were not considered. White circles show the positions of the main fronts (SAF: Subantarctic Front, PF: Polar Front, SACCF: South Antarctic Circumpolar Current Front). Surface chlorophyll concentrations are for December 2009.

during five different periods between 2007 and 2011, transmitting 4498 profiles among which 3388 were usable [see *Guinet et al*., 2013, Table 1]. In our study we used a subset of this data set (1819 profiles from 21 tags; Table S1 in the supporting information) collected in high-chlorophyll regions. The animals were equipped with a multisensors satellite relay data logger, developed by the Sea Mammal Research Unit (UK). Pressure, temperature, and salinity were measured with an accuracy of 2 dbar, 0.02–0.03°C and 0.03–0.05, respectively [*Charrassin et al*., 2008]. In situ fluorescence was measured using the compact in situ fluorometer Cyclops-7 (Turner designs). During the upcasts, fluorescence measurements took place every 2 s and were averaged for a depth interval of 10 m, the mean value being attributed to the depth of the mid interval. Therefore, each profile contained 18 values between 5 and 175 m. Two profiles were transmitted per 24 h. The fluorescence profiles measured during the day were affected by quenching. We corrected this effect using a new method which assumes that chlorophyll is homogenously distributed in the mixed layer and that the quenching effect is negligible at depths below the mixed layer depth (MLD) [*Xing et al*., 2012]. The retrieval of chlorophyll concentrations ([Chl]) from fluorescence measurements provided by different sensors required a careful cross calibration of all the sensors. This was done before deployment by comparison of the fluorescence signal with discrete chlorophyll measurements by high-performance liquid chromatography of samples taken at the same depth [*Xing et al*., 2012]. For the first two deployments, such predeployment calibration was not achieved and a posttreatment utilizing the relative variations of surface chlorophyll concentrations derived from Moderate Resolution Imaging Spectroradiometer (MODIS) was applied [*Guinet et al*., 2013]. For each regions defined below, the mean chlorophyll profile was calculated for periods of 15 days.

2.2. Definitions of the Regions

[6] We have first sorted the data in different regions using the positions of the Subantarctic front (SAF), the polar front (PF), and the Southern Antarctic Circumpolar Current Front (SACCF). The zone between the SAF and the PF is the Polar Front Zone (PFZ), and the region between the PF and the SACCF is the Antarctic Zone (AAZ) (Figure 1). The positions of the fronts were those reported by *Orsi et al*. [1995]. However, for sorting the data north and south of the Polar Front we checked the in situ temperature profiles for the occurrence of a temperature minimum around 200 m. The profile was attributed to the AAZ when the temperature minimum was observed; otherwise, the profile was attributed to the PFZ. We also defined the Kerguelen plateau (KP) region based on the position of the isobath 1000 m reported in the global bathymetry ETOPO2 2 min Global relief (NOAA//ngdc.noaa.gov).

2.3. Mixed Layer Definition and Integration of Chlorophyll

[7] The MLD was defined as the depth where the density anomaly exceeded by 0.03 kg m^{-3} the density anomaly at 15 m. This criterion is similar to that used in MLD climatology [*de Boyer Montégut et al*., 2004]. When the MLD was not detected between 30 and 175m, the MLD was set to 175m. The trapezoidal method was used to derive integrated values of chlorophyll in the mixed layer (Chl_{ML}).

2.4. Photosynthetic Available Radiation

[8] Photosynthetic available radiation at the surface of the ocean ($PAR(0^+)$), average flux for 24 h, was obtained from MODIS-AQUA with a spatial resolution of 9 km and temporal resolution of 8 days. The mean value for the different zones and for periods of 15 days was then calculated.

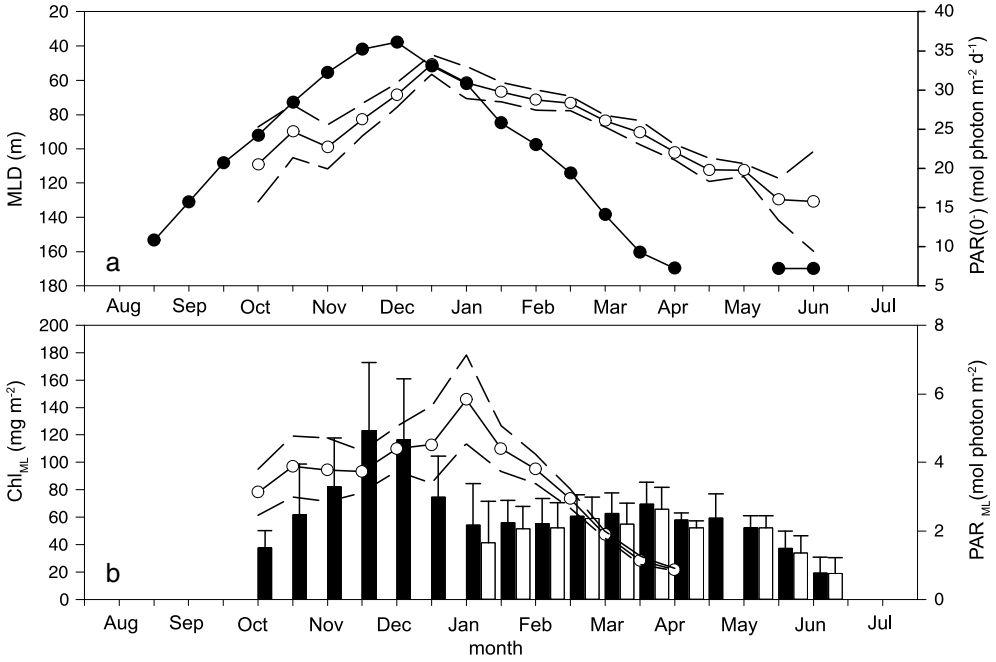

Figure 2. Climatology of PAR, MLD, and integrated chlorophyll for the AAZ. (a) Solid circles denote surface PAR, and open circles denote mean MLD with the confidence interval (99%) given by the dotted lines. (b) Black bars denote the mixed layer integrated chlorophyll (Chl_{ML}) with error bar for confidence interval (99%). White bars are for integrated chlorophyll, corrected for the contribution due to the mixing during deepening ($Chl_{ML,cor}$). Open circles denote mean PAR in the mixed layer ($\overline{PAR_{ML}}$) calculated from equation (1) with the dotted envelop corresponding to the confidence interval (99%).

$PAR(0^-)$ was calculated using a reduction of 7.6% of PAR (0^+) to take into account the radiation diminution when PAR passed through the sea surface [*Morel*, 1991]. The attenuation coefficient of PAR with depth (K_{PAR}) was estimated using the empirical formulation of *Riley* [1956]. This relationship provides similar results to those derived from in situ PAR and Chl profiles in the Crozet region [*Venables and Moore*, 2010]. The mean PAR in the mixed layer was estimated as

$$\overline{PAR_{ML}} = \frac{1}{MLD}\int_0^{MLD} PAR(0^-)\exp^{-K_{PAR}z}dz = \frac{PAR(0^-)}{K_{PAR}MLD}\left(1-\exp^{-K_{PAR}MLD}\right). \quad (1)$$

[9] For given values of $\overline{PAR_{ML}}$, MLD, and $PAR(0^-)$ we also calculated the corresponding [Chl] using Riley's formulation and equation (1).

3. Results

[10] The climatology of profiles of [Chl] and MLD were constructed for the three following zones, PFZ, AAZ, and KP, where the annual coverage was sufficient (Figures S1, S2, and S3).

[11] We detailed here the case of the AAZ. The annual cycle of integrated chlorophyll in the mixed layer (Chl_{ML}) presented four distinct phases (Figure 2). Chl_{ML} increased continuously from the beginning of our observations (mid-October) until mid-December and was associated with a concomitant increase in $PAR(0^-)$ and a shoaling of the mixed layer. During this period, the average PAR over the mixed layer was nearly constant, $\overline{PAR_{ML}} = 3.5$ mol photon m^{-2} d^{-1} (Figures 2b and 3a). In December the bloom stopped (i.e., loss terms exceeded growth) and Chl_{ML} decreased abruptly in early January whereas the mixed layer was shoaling and the surface irradiance started to decrease. The third phase of the seasonal cycle extended from mid-January until May when Chl_{ML} was constant. During this phase, $\overline{PAR_{ML}}$ decreased continuously. The mixed layer deepened, leading to an entrainment of Chl in the newly formed mixed layer. The effect of entrainment on integrated chlorophyll was evaluated (Figure 2b). Entrainment added a minor amount of chlorophyll, and this process can therefore be neglected. Finally, in May, Chl_{ML} decreased to reach winter values.

4. Discussion

[12] During the productive season, all three regions considered in our study are characterized by high [Chl] compared to the surrounding waters [*Fauchereau et al.*, 2011]. Natural iron fertilization enhances phytoplankton growth in these regions. Based on a global analysis of the satellite images of chlorophyll conducted for the entire Southern Ocean between January 1997 and December 2007, the blooms in these regions are characterized by high seasonality [*Thomalla et al.*, 2011]. This gives support to the idea that our data set is representative of a typical mean seasonal cycle in these regions.

[13] During the first phase of the bloom we observed a strong coupling between light availability and integrated biomass. In the absence of other factors than light-limiting phytoplankton growth, a steady state value of $\overline{PAR_{ML}}$ and

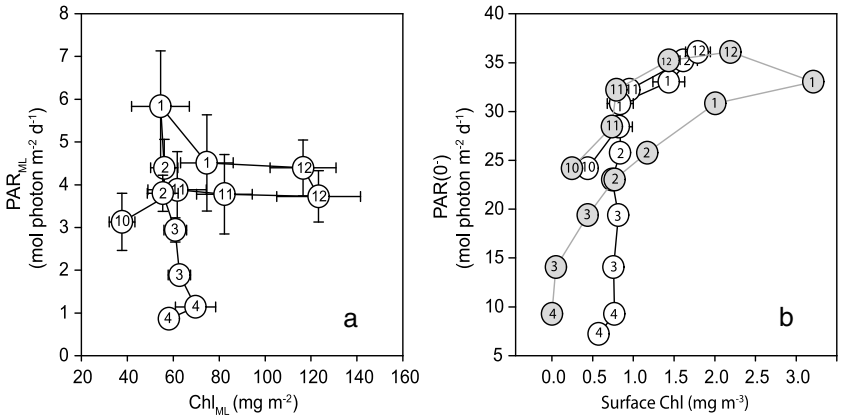

Figure 3. Changes of chlorophyll in the mixed layer as a function of light during the seasonal cycle. (a) Variations of $\overline{\mathrm{PAR_{ML}}}$ and MLD-integrated chlorophyll in the Antarctic zone (AAZ). Error bars are confidence intervals (99%). Numbers within circles denote the month of the year. (b) Variations of the mean concentration of chlorophyll observed in the mixed layer in the Antarctic zone (open circles). Gray circles denote the calculated maximum concentration of chlorophyll that could accumulate if self-shading occurs, assuming the critical value of $\overline{\mathrm{PAR_{ML}}} = 3.5\,\mathrm{mol\ photon\ m^{-2}\ d^{-1}}$. Numbers within circles denote the month of the year.

of $\mathrm{Chl_{ML}}$ can be reached because the light gradient depends on the light attenuation by phytoplankton [*Huisman*, 1999]. In this case, so-called self-shading conditions, for a given $\overline{\mathrm{PAR_{ML}}}$, $\mathrm{Chl_{ML}}$ increases when the MLD decreases and surface irradiance increases. Our conclusion on self-shading control of $\mathrm{Chl_{ML}}$ in iron-fertilized regions of the Southern Ocean are in accordance with previous results of artificial iron fertilization experiments where self-shading was also invoked as the ultimate limit for chlorophyll biomass or inorganic carbon drawdown [*De Baar et al*., 2005]. Our estimate of the critical $\overline{\mathrm{PAR_{ML}}}$ corresponding to self-shading is 3.5 mol photon $\mathrm{m^{-2}\ d^{-1}}$. It represents likely an upper limit because we used 15 days $\mathrm{Chl_{ML}}$ averaged over a wide area with blooms at different stages of development. An estimate of the lower limit of $\overline{\mathrm{PAR_{ML}}}$ could be provided by local and short-term observations. During European Iron Fertilization Experiment [*Smetacek et al*., 2012], the MLD was 97 ± 20 m and [Chl] increased up to 2.5 mg $\mathrm{m^{-3}}$, a concentration reachable considering a critical value of $\overline{\mathrm{PAR_{ML}}} = 2\,\mathrm{mol\ photon\ m^{-2}\ d^{-1}}$ (Figure S4). *Nelson and Smith* [1991] pointed out the role of self-shading in the context of iron fertilization of the Southern Ocean. However, their quantitative conclusion that the stimulation of primary production is minor is now refuted by numerous observations.

[14] The second phase of the seasonal cycle started concomitantly with the $\mathrm{PAR(0^-)}$ decrease. This observation raises the issue whether light limitation could have triggered the decline of the bloom. Considering the threshold $\overline{\mathrm{PAR_{ML}}} = 3.5\,\mathrm{mol}$ mol photon $\mathrm{m^{-2}\ d^{-1}}$ for the limitation of biomass by self-shading and the seasonal variations of $\mathrm{PAR(0^-)}$ and MLD, we calculated the maximum [Chl] that could accumulate in the mixed layer throughout the year (Figure 3b). The comparison with the observed values shows that the bloom stopped well before the maximum of [Chl] = 3 mg $\mathrm{m^{-3}}$ was reached. Consequently, light limitation (i.e., self-shading) could not be the cause of the bloom decline. We note also that soon after the beginning of the decline of the bloom, the light-mixing regime became more favorable with $\overline{\mathrm{PAR_{ML}}}$ increased up to 6 mol photon $\mathrm{m^{-2}\ d^{-1}}$, which is the highest value reached throughout the season. This is due to the abrupt decrease of light attenuation related to [Chl] decrease, which largely compensates the effect of the $\mathrm{PAR(0^-)}$ decrease and of the MLD deepening, on the gradient of light. The occurrence of more favorable light conditions did not modify the decreasing trend of $\mathrm{Chl_{ML}}$. Therefore, another factor aside from light caused the end of the bloom and the decrease of $\mathrm{Chl_{ML}}$. It is possible that the occurrence of limiting concentrations of silicic acid for diatoms [*Mosseri et al*., 2008] have decreased the growth rate below the loss rates (mortality and grazing), but alternative hypothesis favoring the increase of loss rate (e.g., grazing) cannot be ruled out. Physiological changes could also have altered the fluorescence yield of the cells but, it is unlikely that it could account for the large decrease of roughly 75% of the $\mathrm{Chl_{ML}}$ observed between the second half of December and the end of January. During this period of the year, the fluorescence per unit of chlorophyll derived from satellite shows little variations [*Westberry et al*., 2013].

[15] Following the collapse of the spring bloom steady state $\mathrm{Chl_{ML}}$ were observed. A planktonic ecosystem has emerged where significant phytoplankton growth balanced grazing and sinking. As observed in similar fertilized environments [*Poulton et al*., 2007; *Quéguiner*, 2013], the phytoplankton community could contain nonsiliceous organisms (e.g., Phaeocystis) and slow-growing diatoms. This community was likely adapted to summer and fall environmental conditions (light and nutrients). Finally, in June, $\mathrm{Chl_{ML}}$ decreased coinciding with $\overline{\mathrm{PAR_{ML}}} = 1\,\mathrm{mol\ photon\ m^{-2}\ d^{-1}}$ which could be the irradiance threshold that limits the autumnal phytoplankton community.

[16] Another approach that has been widely used to address the role of light-mixing regime on dynamics of phytoplankton biomass is the comparison of the MLD to the critical depth Z_{cr}, above which integrated gain and loss of biomass are balanced. *Sverdrup* [1953] derived an analytical expression linking the incident irradiance, Z_{cr}, and the compensation light I_c required for photosynthesis to balance loss rates. The latter was difficult to estimate because it must account for any loss terms and not only for phytoplankton or community respiration [*Smetacek and Passlow*, 1990]. *Nelson and Smith* [1991] revisited

Sverdrup's theory for the Southern Ocean and proposed $I_c = 3$ mol photon m^{-2} d^{-1} as the best empirical estimate. More recently, $I_c = 1.4$ mol photon m^{-2} d^{-1} was proposed for a high-chlorophyll region of the Southern Ocean [*Venables and Moore*, 2010]. We have used this latter value of I_c as a first estimate to compute Z_{cr} in our region (Figure S5). From mid-October to March, Z_{cr} is well below the MLD suggesting that the light-mixing regime is favorable for net growth of phytoplankton, confirming similar conclusions obtained with a different approach [*Venables and Moore*, 2010]. The onset of the bloom should have occurred earlier than mid-October. Due to the lack of elephant seal's data for this period, we have estimated Z_{cr} based on incident light and MLD climatology [*de Boyer Montégut et al*., 2004] (Figure S5). At the spatial and temporal resolutions we considered, our observations did not contradict Sverdrup's model for the initiation of the bloom. However, a higher-resolution data set will be required to examine alternative explanations like the decoupling theory [*Behrenfeld*, 2010], the role of mixing versus mixed layers [*Chiswell*, 2011; *Taylor and Ferrari*, 2011] or of instabilities in surface currents [*Mahadevan et al*., 2012].

[17] **Acknowledgments.** This project was funded by the ANR, CNES, and IPEV. Analyses and visualizations of satellite chlorophyll used in this paper were produced with the Giovanni online data system and developed and maintained by the NASA GES DISC. We also thank Ingrid Obernosterer, Ian Salter, and Marina Levy for their careful reading of the manuscript and two anonymous reviewers for their constructive comments.

[18] The Editor thanks two anonymous reviewers for their assistance in evaluating this paper.

References

Allison, D. B., D. Stramski, and B. G. Mitchell (2010), Seasonal and interannual variability of particulate organic carbon within the Southern Ocean from satellite ocean color observations, *J. Geophys. Res.*, *115*, C06002, doi:10.1029/2009JC005347.

Arrigo, K. R., G. L. van Dijken, and S. Bushinsky (2008), Primary production in the Southern Ocean, 1997–2006, *J. Geophys. Res.*, *113*, C08004, doi:10.1029/2007JC004551.

Behrenfeld, M. J. (2010), Abandoning Sverdrup's critical depth hypothesis on phytoplankton blooms, *Ecology*, *91*(4), 977–989.

Blain, S., et al. (2007), Effect of natural iron fertilisation on carbon sequestration in the Southern Ocean, *Nature*, *446*(7139), 1070–1075, doi:10.1038/nature05700.

Boyd, P. W. (2002), Environmental factors controlling phytoplankton processes in the Southern ocean, *J. Phycol.*, *38*, 844–861.

Boyd, P. W., et al. (2007), Mesoscale iron enrichment experiments 1993–2005: Synthesis and future directions, *Science*, *315*, 612–617, doi:10.1126/science.1131669.

Charrassin, J.-B., et al. (2008), Southern Ocean frontal structure and sea-ice formation rates revealed by elephant seals, *Proc. Natl. Acad. Sci.*, *105*(33), 11,634–11,639, doi:10.1073/pnas.0800790105.

Chiswell, S. (2011), Annual cycles and spring blooms in phytoplankton: Don't abandon Sverdrup completely, *Mar. Ecol. Prog. Ser.*, *443*, 39–50, doi:10.3354/meps09453.

De Baar, H. J. W., et al. (2005), Synthesis of iron fertilization experiments: From the iron age in the age of enlightenment, *J. Geophys. Res.*, *110*, C09S16, doi:10.1029/2004GC002601.

De Boyer Montégut, C., G. Madec, A. S. Fischer, A. Lazar, and D. Iudicone (2004), Mixed layer depth over the global ocean: An examination of profile data and a profile-based climatology, *J. Geophys. Res.*, *109*, C12003, doi:10.1029/2004JC002378.

Fauchereau, N., A. Tagliabue, L. Bopp, and P. M. S. Monteiro (2011), The response of phytoplankton biomass to transient mixing events in the Southern Ocean, *Geophys. Res. Lett.*, *38*, L17601, doi:10.1029/2011GL048498.

Guinet, C., et al. (2013), Calibration procedures and first data set of Southern Ocean chlorophyll *a* profiles collected by elephant seal equipped with a newly developed CTD-fluorescence tags, *Earth Syst. Sci. data*, *5*, 15–29, doi:10.5194/essd-5-15-2013.

Huisman, J. (1999), Population dynamics of light-limited phytoplankton: Microcosm experiments, *Ecology*, *80*(1), 202–210, doi:10.1890/0012-9658(1999)080[0202:PDOLLP]2.0.CO;2.

Lovenduski, N. S., and N. Gruber (2005), Impact of the Southern Annular Mode on Southern Ocean circulation and biology, *Geophys. Res. Lett.*, *32*, L11603, doi:10.1029/2005GL022727.

Mahadevan, A., E. D'Asaro, C. Lee, and M. J. Perry (2012), Eddy-driven stratification initiates North Atlantic spring phytoplankton blooms, *Science*, *337*(6090), 54–58, doi:10.1126/science.1218740.

Marinov, I., A. Gnanadesikan, J. R. Toggweiler, and J. L. Sarmiento (2006), The Southern Ocean biogeochemical divide, *Nature*, *441*, 964–967, doi:10.1038/nature04883.

Morel, A. (1991), Light and marine photosynthesis: A spectral model with geochemical and climatological implications, *Prog.Oceanogr.*, *26*, 263–306.

Mosseri, J., B. Quéguiner, L. Armand, and V. Cornet-Barthaux (2008), Impact of iron on silicon utilization by diatoms in the Southern Ocean: A case study of Si/N cycle decoupling in a naturally iron-enriched area, *Deep Sea Res. Part II*, *55*(5–7), 801, doi:10.1016/j.dsr2.2007.12.003.

Nelson, D. M., and W. O. Smith (1991), Sverdrup revisited: Critical depths, maximum chlorophyll levels, and the control of Southern Ocean productivity by the irradiance-mixing regime, *Limnol. Oceanogr.*, *36*(8), 1650–1661.

Orsi, A. H., I. T. Whitworth, and J. W. D. Nowlin (1995), On the meridional extent and fronts of the Antarctic Circumpolar Current, *Deep Sea Res. Part I*, *42*(5), 641.

Pollard, R. T., et al. (2009), Southern Ocean deep-water carbon export enhanced by natural iron fertilization, *Nature*, *457*(7229), 577–580, doi:10.1038/nature07716.

Poulton, A. J., C. M. Moore, S. Seeyave, M. I. Lucas, S. Fielding, and P. Ward (2007), Phytoplankton community composition around the Crozet Plateau, with emphasis on diatoms and Phaeocystis, *Deep Sea Res. Part II*, *54*, 2085–2015, doi:10.1016/j.dsr2.2007.06.010.

Quéguiner, B. (2013), Iron fertilization and the structure of planktonic communities in high nutrient regions of the Southern Ocean, *Deep Sea Res. Part II*, *90*, 43–54, doi:10.1016/j.dsr2.2012.07.024.

Riley, G. A. (1956), Oceanography of Long Island Sound, 1952–1954. Production and utilization of organic matter, *Bull. Bingham. Oceanogr. Collect.*, *15*, 324–343.

Sallée, J. B., K. G. Speer, and S. R. Rintoul (2010), Zonally asymmetric response of the Southern Ocean mixed-layer depth to the Southern Annular Mode, *Nat. Geosci.*, *3*(4), 273–279, doi:10.1038/ngeo812.

Sigman, D. M., M. P. Hain, and G. H. Haug (2010), The polar ocean and glacial cycles in atmospheric CO_2 concentration, *Nature*, *466*(7302), 47–55, doi:10.1038/nature09149.

Smetacek, V., and U. Passlow (1990), Spring bloom initiation and Sverdrup's critical-depth model, *Limnol. Oceanogr.*, *35*(1), 228–234.

Smetacek, V., et al. (2012), Deep carbon export from a Southern Ocean iron-fertilized diatom bloom, *Nature*, *487*(7407), 313–319, doi:10.1038/nature11229.

Sverdrup, H. U. (1953), On conditions for the vernal blooming of phytoplankton, *J. Conseil Int.Explor. la Mer.*, 287–295.

Taylor, J. R., and R. Ferrari (2011), Shutdown of turbulent convection as a new criterion for the onset of spring phytoplankton blooms, *Limnol. Oceanogr.*, *56*(6), 2293–2307, doi:10.4319/lo.2011.56.6.2293.

Thomalla, S. J., N. Fauchereau, S. Swart, and P. M. S. Monteiro (2011), Regional scale characteristics of the seasonal cycle of chlorophyll in the Southern Ocean, *Biogeosciences*, *8*(10), 2849–2866, doi:10.5194/bg-8-2849-2011.

Venables, H., and C. M. Moore (2010), Phytoplankton and light limitation in the Southern Ocean: Learning from high-nutrient, high-chlorophyll areas, *J. Geophys. Res.*, *115*, C02015, doi:10.1029/2009JC005361.

Westberry, T. K., M. J. Behrenfeld, A. J. Milligan, and S. C. Doney (2013), Retrospective satellite ocean color analysis of purposeful and natural ocean iron fertilization, *Deep Sea Res. Part I*, *73*, 1–16, doi:10.1016/j.dsr.2012.11.010.

Xing, X., H. Claustre, S. Blain, F. D'Ortenzio, D. Antoine, J. Ras, and C. Guinet (2012), Quenching correction for in vivo chlorophyll fluorescence acquired by autonomous platforms: A case study with instrumented elephant seals in the Kerguelen region (Southern Ocean), *Limnol. Oceanogr. Methods*, *10*, 483–495, doi:10.4319/lom.2012.10.483.